Journal of Geophysical Research: Oceans

RESEARCH ARTICLE
10.1029/2018JC013932

Key Points:
- Subsurface dissolved iron concentrations around the southern Kerguelen plateau were more variable than surface concentrations
- Sustained upwelling of subsurface iron is the most likely mechanism supplying iron to the persistent phytoplankton blooms in the region
- Horizontal advection of subsurface iron and upwelling associated with the Antarctic Divergence combine to create a biological hot spot

Supporting Information:
- Supporting Information S1

Correspondence to:
C. Schallenberg,
christina.schallenberg@utas.edu.au

Citation:
Schallenberg, C., Bestley, S., Klocker, A., Trull, T. W., Davies, D. M., Gault-Ringold, M., et al. (2018). Sustained upwelling of subsurface iron supplies seasonally persistent phytoplankton blooms around the southern Kerguelen plateau, Southern Ocean. *Journal of Geophysical Research: Oceans*, *123*, 5986–6003. https://doi.org/10.1029/2018JC013932

Received 22 FEB 2018
Accepted 26 JUN 2018
Accepted article online 6 AUG 2018
Published online 29 AUG 2018

Sustained Upwelling of Subsurface Iron Supplies Seasonally Persistent Phytoplankton Blooms Around the Southern Kerguelen Plateau, Southern Ocean

Christina Schallenberg[1], Sophie Bestley[2,3], Andreas Klocker[2,4], Thomas W. Trull[1,3], Diana M. Davies[1,3], Melanie Gault-Ringold[1], Ruth Eriksen[3], Nicholas P. Roden[1], Sylvia G. Sander[5,6], Michael Sumner[7], Ashley T. Townsend[8], Pier van der Merwe[1], Karen Westwood[1,7], Kathrin Wuttig[1], and Andrew Bowie[1,2]

[1]Antarctic Climate and Ecosystems Cooperative Research Centre, University of Tasmania, Hobart, Tasmania, Australia, [2]Institute for Marine and Antarctic Studies, University of Tasmania, Hobart, Tasmania, Australia, [3]CSIRO Oceans and Atmosphere, Castray Esplanade, Hobart, Tasmania, Australia, [4]Australian Research Council Centre of Excellence for Climate System Science, University of Tasmania, Hobart, Tasmania, Australia, [5]NIWA/University of Otago Research Centre Oceanography, University of Otago, Dunedin, New Zealand, [6]Now at Marine Environmental Studies Laboratory, IAEA-NAEL, Monaco, Principality of Monaco, [7]Australian Antarctic Division, Department of the Environment and Energy, Kingston, Tasmania, Australia, [8]Central Science Laboratory, University of Tasmania, Hobart, Tasmania, Australia

Abstract Although the supply of iron generally limits phytoplankton productivity in the Southern Ocean, substantial seasonal blooms are observed over and downstream of the Kerguelen plateau in the Indian sector of the Southern Ocean. Surprisingly, of the oceanic blooms, those associated with the deeper southern plateau last much longer (~3 months) than the northern bloom (~1-month downstream of northern plateau). In this study, iron supply mechanisms around the southern plateau were investigated, obtaining profiles of dissolved iron (<0.2 μm, dFe) to 2,000-m deep at 25 stations during austral summer 2016. The dFe concentrations in surface waters (≤100-m depth) ranged from below the detection limit (DL, median of 0.026 nmol/kg) to 0.34 nmol/kg near the Antarctic shelf, with almost half the data points below detection. These low and—with few exceptions—largely spatially invariant concentrations, presumably driven by seasonal drawdown of this essential micronutrient by phytoplankton, could not explain observed patterns in chlorophyll *a*. In contrast, dFe concentrations (0.05–1.27 nmol/kg) in subsurface waters (100–800 m) showed strong spatial variations that can explain bloom patterns around the southern Kerguelen plateau when considered in the context of frontal locations and associated frontal processes, including upwelling, that may increase the upward supply of dFe in the region. This sustained vertical dFe supply distinguishes the southern blooms from the bloom downstream of the northern Kerguelen plateau and explains their persistence through the season.

Plain Language Summary Over much of the Southern Ocean, phytoplankton productivity is hampered by a lack of dissolved iron, an essential micronutrient for phytoplankton. However, there are areas where phytoplankton thrive, and these are often associated with topographic features. For example, a large phytoplankton bloom develops each year downstream of the northern Kerguelen plateau. This bloom peaks around December and subsequently declines. It receives its iron supply mainly from the sediments on the shallow plateau, carried downstream in surface waters with the currents. There are also blooms near the much deeper (>1,000 m) southern Kerguelen plateau, but the supply of iron to these blooms was poorly understood until now. These blooms persist through the growing season and thus outlast the bloom downstream of the northern Kerguelen plateau. Our study results indicate that the southern blooms receive their iron from the subsurface, and that the source of the iron likely includes Antarctic shelf sediments and remineralization of sinking material. Localized upwelling associated with the wind and current patterns in the region brings this subsurface iron to the surface, where it fuels phytoplankton growth. The key to the longevity of the blooms thus appears to be the combination of a subsurface iron source and persistent upwelling.

1. Introduction

Phytoplankton growth in the Southern Ocean is limited by an insufficient supply of iron, with the consequence that macronutrients are not consumed to the same extent as in other oceanic regions (de Baar et al., 1995; Martin, 1990; Moore et al., 2002). The resulting high-nutrient, low-chlorophyll condition is a

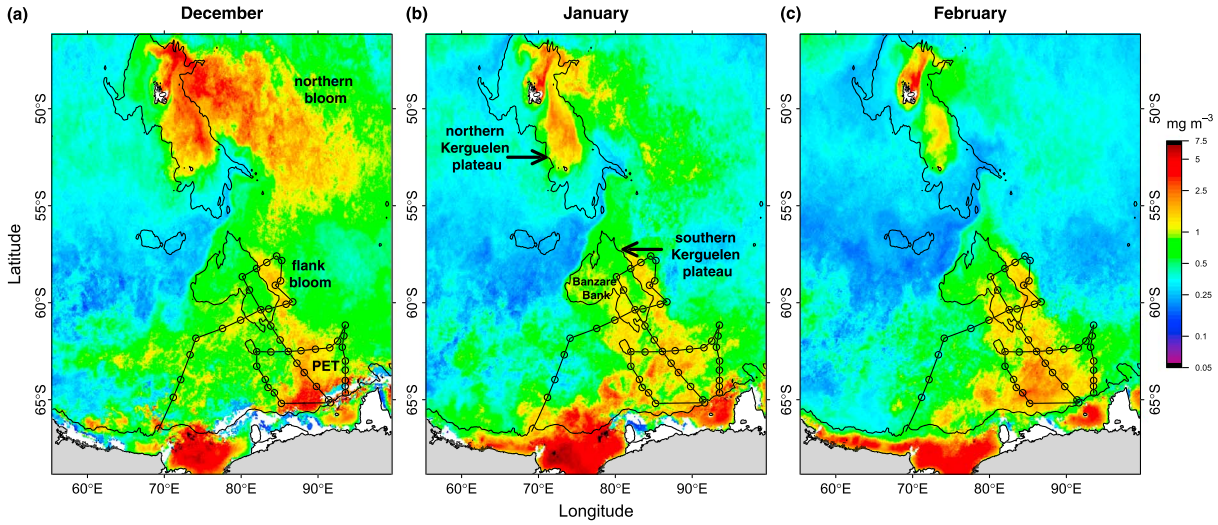

Figure 1. Chl *a* climatologies for the Kerguelen region, calculated using the Johnson et al. (2013) chl *a* algorithm and MODIS satellite data (years 2002–2017). The 2,000-m isobaths (gray) and *K* axis cruise track (black line with circles indicating station locations) are also shown. Main bloom locations and the two different plateaus are indicated. MODIS = Moderate Resolution Imaging Spectroradiometer.

diagnostic for iron limitation that reveals an underlying potential for greater carbon uptake in the presence of increased micronutrient supply. Indeed, the Southern Ocean has a large influence on the global carbon cycle, both via physical and biological processes, with carbon sequestration by phytoplankton directly linked to iron supply (Boyd et al., 2007; Jickells et al., 2005; Sigman & Boyle, 2000).

Over much of the open Southern Ocean, deep winter mixing supplies the bulk of the iron available for phytoplankton growth (Tagliabue et al., 2014), but sedimentary sources become important near islands and continental shelves (Blain et al., 2008; Graham et al., 2015; Robinson et al., 2016; Wadley et al., 2014). Melting sea ice also constitutes a seasonally important iron source (Lannuzel et al., 2016; Schallenberg et al., 2016; Sedwick & DiTullio, 1997), and there is evidence that chlorophyll *a* (chl *a*) is enhanced near certain fronts (Moore & Abbott, 2002; Tynan, 1998), presumably due to upwelling of iron-rich waters.

Examination of chl *a* climatologies for the Indian sector of the Southern Ocean reveals substantial phytoplankton blooms over and in the vicinity of the submarine Kerguelen plateau (Figure 1). However, not all the iron sources supporting these blooms are well understood. Two distinct blooms are associated with the northern Kerguelen plateau: a sustained bloom over the shallow plateau and a spring bloom in deep waters downstream (to the east) of the plateau. The phytoplankton bloom over the plateau lasts through the whole austral summer season. This is thought to be sustained by vertical iron supply from the shallow shelf sediments (<500 m), supplied by elevated vertical diffusivity due to internal tides and deep winter mixing (Blain et al., 2008; Bowie et al., 2015; Mongin et al., 2008). In addition, island sources of iron resulting from glacial melting during the summer may also play an important role in sustaining the bloom (van der Merwe et al., 2015). Downstream, east of the northern Kerguelen plateau, a large bloom develops every year, although its spatial extent varies (Mongin et al., 2009; Robinson et al., 2016). This bloom is most evident in the December chl *a* climatology (Figure 1) and, unlike the bloom over the northern plateau, it fades in the subsequent months. Budget calculations as well as modeling studies indicate that this downstream bloom is largely supplied by lateral advection of iron in surface waters from the northern Kerguelen plateau (Bowie et al., 2015; D'Ovidio et al., 2015; Grenier et al., 2015; Mongin et al., 2009), although some questions remain regarding the year-to-year variability of the bloom's extent (Robinson et al., 2016).

Around the southern Kerguelen plateau, sustained phytoplankton blooms are observed along the eastern flank as far north as 57°S, as well as over the Princess Elizabeth Trough (PET) to the south-east of the plateau (i.e., south of 62°S, 83–95°E, Figure 1). The southwestern flank of the bank (near 62°S, 80°E) is also an area of elevated chl *a* later in the season. Surprisingly, these sustained blooms are found in deep water (≥3,000 m) and at considerable distance from shallow iron sources (the southern Kerguelen plateau is predominantly deeper than 1,000 m, thus not likely constituting a direct iron source to surface waters). In the case of the

PET bloom, horizontal advection at the surface has been proposed to supply iron and/or phytoplankton from the nearby Antarctic continental shelf, as a strong northerly current persists near 85°E (Rintoul et al., 2008). However, if lateral advection of surface waters were the main driver of iron supply, as proposed for the bloom downstream of the northern Kerguelen plateau, why does the PET bloom persist through the season while the oceanic bloom downstream of the northern Kerguelen plateau does not? This contrast in longevity deserves further exploration and was one motivation for this study.

Furthermore, lateral advection of iron from the Antarctic shelf does not clearly explain the bloom north of the PET, that is, along the southeastern flank of the southern Kerguelen plateau. For this area, Sokolov and Rintoul (2007) proposed that vertical motion, resulting from the main current flow interacting with topography, could supply iron. However, as far as we know, iron concentrations have never been directly measured within this region.

In this paper, dissolved iron (dFe) data are integrated with in situ information on primary productivity (integrated chl *a* and nitrogen stable isotopes) into the broader context provided by satellite remote sensing and the *K* axis oceanographic survey (named in reference to the Kerguelen axis). We use these results to evaluate existing hypotheses regarding iron supply and ultimately propose a new hypothesis for the mechanisms supporting the extensive and sustained primary production in the region.

2. Methods

2.1. Oceanographic Setting and Sampling of the Southern Kerguelen Plateau

A research voyage to the southern Kerguelen plateau in the Indian sector of the Southern Ocean was undertaken aboard the RV *Aurora Australis* in January–February 2016. The sampling region (72–94°E, 58–66°S) is seasonally ice covered with the exception of two stations at the northeast corner of the survey. Only a small fraction of the southern Kerguelen plateau over Banzare Bank lies shallower than 1,000 m, with the main part being 1,200 to 2,000-m deep. The *K* axis survey covered waters ranging in depth from >3,000 m within the PET and west of the plateau to near 1,200 m on the Antarctic slope and 1,350 m on Banzare Bank.

The Kerguelen plateau presents a major barrier to the eastward flowing Antarctic Circumpolar Current (ACC), diverting the flow around the topography. Between the northern and southern plateaus lies the Fawn Trough (2,600-m sill depth), through which ~30% of the ACC is funneled (Park et al., 2009; Vivier et al., 2015). The regionally named Fawn Trough Current (FTC) skirts the northwestern flank of the southern Kerguelen plateau before turning southeasterly further downstream (Figure 2a; see McCartney & Donohue, 2007; Park et al., 2009). South of the southern Kerguelen plateau the ACC also continues eastward through the PET (3,600-m sill depth; see Heywood et al., 1999; McCartney & Donohue, 2007; Sparrow et al., 1996). The two major ACC southerly fronts (the southern ACC front, sACCf, and the southern boundary, SB) tend to be colocated west of 85°E and separate after a sharp turn to the north (Figure 2a; see Bestley et al., 2018). They then flow northward up the eastern flank of the plateau before retroflecting downstream and joining the FTC (Aoki et al., 2008; Orsi et al., 1995; Roquet et al., 2009). In contrast, transport over the southern Kerguelen plateau itself is sluggish (Bestley et al., 2018).

Although the main survey domain within the PET region had been ice free for >4 weeks at the time of sampling, seasonal sea ice was still present at Stations 18–20 (Figure 2b). Ice retreat in that area occurred about 4–5 weeks later in 2015/2016 compared to the long-term climatology, and the late presence of sea ice could have altered surface flows there (Bestley et al., 2018). Sea ice advected by winds was also encountered at Station 21.

Oceanic profiles (conductivity, temperature, depth, hereafter CTD) were collected at 47 stations using Seabird SBE9plus instrumentation (Bestley et al., 2018), with associated sampling conducted from a 24-bottle rosette frame equipped with 10 L Niskin bottles. Oceanic sampling took place between 22 January and 16 February, 2016. CTD sensors were calibrated with onboard measurements of oxygen and salinity on discrete samples from the Niskin bottles (Rosenberg & Eriksen, 2016).

At 25 stations, an autonomous trace-metal clean rosette system (TMR), equipped with 12 × 5 L Teflon-lined Go-Flo bottles, was deployed from the stern of the RV *Aurora Australis* to collect samples for trace element analysis, as described in Bowie et al. (2009). The TMR has a polyurethane powder-coated aluminum frame with sacrificial Mg anodes and was weighted with plastic-coated lead weights. It was attached to 6,000 m

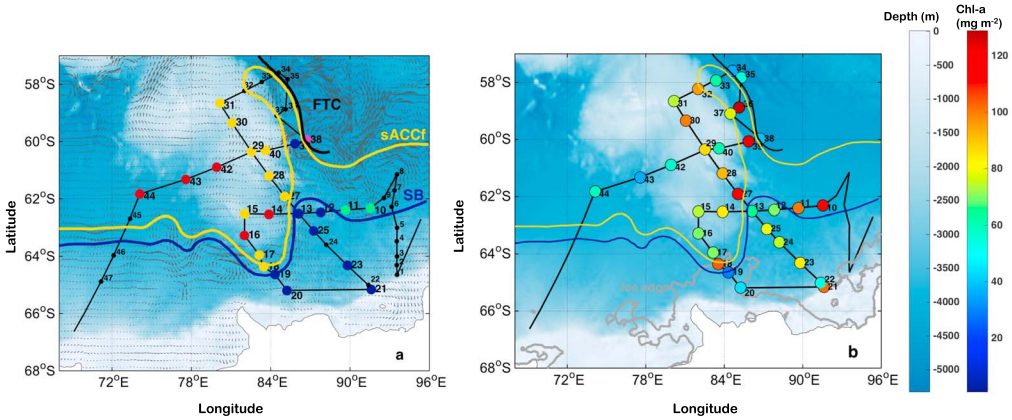

Figure 2. Panels show the cruise track with TMR station locations on the region's bathymetry (colored circles; black circles indicate stations that were not sampled with the TMR). Stations in Figure 2a are colored according to oceanic zones, defined based on physical water properties and location relative to the major fronts. Blue is below the southern boundary (SB), green stations are in a southerly water mass between the south Antarctic Circumpolar Current front (sACCf) and SB, yellow is a plateau-associated water mass, and red is above the sACCf; see Bestley et al. (2018) for details. Average geostrophic currents for 25/26 January (i.e., the dates when Stations 10 and 11 were sampled) are indicated by gray arrows. The Fawn Trough Current (FTC) is indicated in black. Figure 2b shows depth-integrated chlorophyll *a* (calculated based on HPLC measurements); the location of the ice edge on 2 February is indicated in gray. TMR = trace-metal clean rosette system; HPLC = high-performance liquid chromatography.

of Dyneema™ rope with a stainless steel (316 grade) shackle. All trace metal sampling followed international GEOTRACES protocols (Cutter et al., 2010) and was completed between 25 January and 14 February 2016.

2.2. HPLC Chl *a*

Seawater samples (~2 L) from Niskin bottles mounted on the main CTD rosette system were taken at six depths in the photic zone, with individual sample depths determined based on the real-time fluorescence trace of each CTD profile. Samples were kept away from light sources and filtered onto 13-mm Advantec GF/F filters (0.6-μm nominal pore size) under vacuum (<0.5 atm) and then blotted dry and stored in 1.5-ml cryotubes in liquid nitrogen. In the laboratory, chl *a* was extracted using high-performance liquid chromatography (HPLC) following a modified method of Mock and Hoch (2005), described in detail in Wright et al. (2010). Integrated chl *a* was calculated by assuming zero chl *a* at 120 m, interpolating the data with respect to depth using a piecewise cubic hermite interpolating polynomial (in MATLAB), and integrating the resulting depth profiles from 0 to 120 m.

2.3. Satellite Chl *a*

Daily satellite Remote Sensing Reflectance data were obtained from the Moderate Resolution Imaging Spectroradiometer Aqua satellite as distributed by National Aeronautics and Space Administration (Level 3 binned, 4.6-km resolution; https://oceandata.sci.gsfc.nasa.gov/MODIS-Aqua/L3BIN/). Data for the years 2002–2017 were processed with the chl *a* algorithm of Johnson et al. (2013), which yields improved estimates in the Southern Ocean compared to the OC3 algorithm. Climatological mean and standard deviation (SD) fields for select time periods were calculated using log-transformed chl *a* data. The centered chl *a* anomaly for the voyage duration (i.e., 18 January to 18 February) relative to the long-term climatology for that period was calculated by subtracting the climatological field from that of the observation period and normalizing to the SD. Satellite products were accessed using the libraries *raadtools* (Sumner, 2016) and *roc* (Sumner, 2017) for the freely available R software (R Core Team, 2016).

2.4. Nitrogen Stable Isotopes

Particles were filtered from the ship's underway water supply (5-m depth, 1.4- to 1.5-atm filtration pressure, up to 300 L) through a 1-mm mesh (47-mm diameter) to remove zooplankton, and sequentially through 210-μm mesh (Nitex) and 1.2-μm silver filters (Sterlitech). Initially, only the 1.2- to 210-μm fraction was collected for analysis. Later it became obvious that larger diatoms were being excluded, especially *Rhizosolenia* mats (at

Station 43 the mats were so abundant at 50 m that a sample was obtained from a Niskin bottle [8.5 L]), and the 210-μm mesh samples were therefore also analyzed, by transferring these particles to 1.2-μm silver filters. Zooplankton were very sparse (visible on drying at 60 °C) and were picked off before analysis.

Isotopic analysis was by inline combustion continuous flow Isotope Ratio Mass Spectrometry at Australian Nuclear Science and Technology Organization, Lucas Heights. The combustion was via a Thermo Fisher Flash 2000HT Elemental Analyzer, and the gases transferred to a Thermo Fisher Delta V plus Isotope Ratio Mass Spectrometer through a Thermo Fisher Conflo IV. The data are reported relative to International Atomic Energy Agency secondary certified standards. Standard error of analysis to 1 SD was ±0.3 mil.

2.5. Dissolved Iron

Go-Flo bottles were transferred from the TMR to a trace-element clean laboratory container on the aft deck. Samples for trace element analyses, including dFe, were filtered through acid-cleaned 0.2-μm cartridge filters (Pall Acropak) under constant airflow from several International Organization for Standardization (ISO) class five high-efficiency particulate air units. All plastic ware was acid-cleaned prior to use, following GEOTRACES protocols (Cutter et al., 2010). Samples were collected into low-density polyethylene bottles, acidified immediately to pH 1.7 with Seastar Baseline hydrochloric acid, double-bagged and stored at room temperature until analysis onshore.

A subset of salinity samples (n = 124) was also taken from Go-Flo bottles to check whether bottles had closed at the expected depths and/or whether there were problems with leaking. Salinity samples were compared to CTD salinities, and samples where measured salinity did not match the respective CTD salinity (n = 9) were flagged as suspect and are not included in this analysis. Note that salinity checks were predominantly performed on Go-Flo bottles that were suspicious (e.g., leaking), so they do not represent a random set of samples.

Samples for dFe analysis (40 mL) were preconcentrated offline (factor 40) on a SeaFAST S2 pico (ESI, Elemental Scientific, USA) flow injection system with a Nobias Chelate-PA1 column. The setup is similar to that of Lagerström et al. (2013), with modifications as follows: Samples were eluted from the column in 10% distilled nitric acid (HNO_3), with calibration based on the method of standard additions in seawater (made using multielement standards in a 10% HNO_3 matrix, rather than an hydrochloric acid matrix). Seawater standards were preconcentrated on the SeaFAST in the same way as seawater samples. Preconcentrated samples were analyzed using Sector Field Inductively Coupled Plasma Mass Spectrometry (SF-ICP-MS, Thermo Fisher Scientific, Inc.). Data were blank corrected by subtracting an average acidified Milli-Q blank (range 0.03–0.17 nmol/kg) that was preconcentrated on the SeaFAST in the same way as the samples and seawater standards (starting volume 40 ml).

The dFe DL for a given analysis run on the SeaFAST/SF-ICP-MS was calculated as 3 × SD of the Milli-Q blank on that run. DL ranged from 0.016 to 0.067 nmol/kg, with a median of 0.026 nmol/kg (n = 12). DLs were applied such that data from below the DL were replaced with the DL value from the respective run, that is, no *global* DL was applied for the whole cruise. GEOTRACES reference materials were analyzed along with samples, and results were in good agreement with consensus values: SAFe D1 was measured at 0.69 ± 0.05 nmol/kg (n = 7; consensus value = 0.67 ±0.04 nmol/kg), SAFe S was measured at 0.086 ± 0.024 nmol/kg (n = 3, consensus value = 0.093 ± 0.008) and GD was measured at 1.02 ± 0.01 nmol/kg (n = 6; consensus value = 1.00 ± 0.1 nmol/kg). Integrated dFe was estimated by linearly interpolating dFe with respect to depth and integrating the resulting depth profiles between 20 and 750 m.

3. Results

In what follows we first present results pertaining to the chl *a* distributions around the Kerguelen plateau, comparing climatological satellite data to the situation that was encountered on the *K* axis voyage in austral summer of 2016. Next, we present dFe data, with an emphasis on stations where high chl *a* concentrations were encountered. These observations are then put in context with nitrogen stable isotope data.

3.1. Chl *a* Climatology Around the Kerguelen Plateau

Monthly regional satellite chl *a* climatologies illustrate how the phytoplankton blooms associated with the northern and southern Kerguelen plateau behave differently over the summer season (Figure 1; see also Figure S1 in the supporting information). The large bloom downstream of the northern plateau reaches its

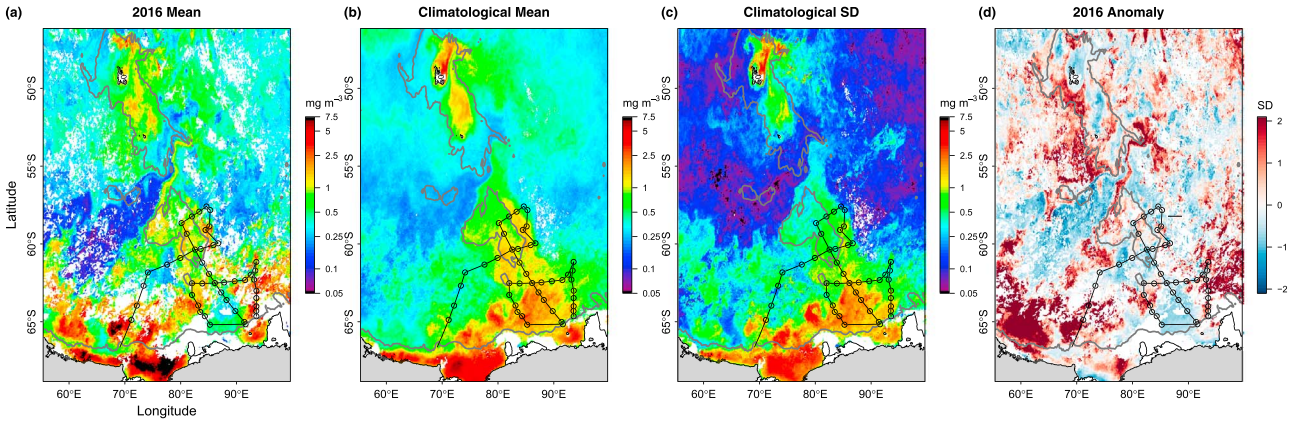

Figure 3. Chl *a* maps for the time period of in situ sampling (18 January to 18 February 2016) on the research cruise. Panels are as follows: (a) the mean for 2016, that is, the year when the cruise took place; (b) the climatological mean and (c) its standard deviation; and (d) the centered anomaly of the observations in 2016 relative to the climatology. SD = standard deviation.

maximum extent in December and subsequently declines, while a smaller bloom persists over the northern plateau throughout the season, with highest chl *a* concentrations observed northeast of Kerguelen Island. Over the southern plateau, chl *a* concentrations do not reach as high as in the northern blooms (mainly <1 mg chl *a*/m^3 over the southern plateau compared to >2.5 mg chl *a*/m^3 in the northern blooms). However, persistently high chl *a* is observed on the eastern flank of the southern plateau (~2 mg chl *a*/m^3) and also over the deep PET to the southeast of the plateau (up to 2.5 mg chl *a*/m^3). In contrast to the bloom downstream of the northern plateau, the blooms associated with the southern plateau (hereafter, named as the flank and PET blooms) are sustained throughout the growing season December through February (Figure 1).

3.2. Observed Chl *a* During the Voyage Period in Austral Summer 2016

The satellite chl *a* observations for the voyage duration in 2016 (Figure 3a) were largely consistent with the climatology for that same period (Figure 3b) with regards to spatial patterns in chl *a* within the region of interest. An examination of the centered anomalies (Figure 3d) shows that chl *a* was overall somewhat high in 2016 but not significant in relation to what has historically been observed (i.e., few dark red areas, indicating $\geq +2$ SD). These areas were mainly west of the northern plateau and northwest of Prydz Bay (i.e., outside the survey region), as well as in the southeast survey area. The area of historically lowest chl *a* upstream of the Fawn Trough was notably even lower in 2016. Some of the regions with historically high chl *a* did display weak negative anomalies in 2016 (<-1 SD). These include discrete areas on the northern Kerguelen plateau as well as the center of the PET bloom. However, none of the sampled areas showed anomalies >2 SD (see also Figure S2), indicating that we encountered a reasonably normal regime during the *K* axis voyage.

Depth-integrated chl *a* concentrations based on HPLC measurements (Figure 2b) showed patterns that were broadly consistent with satellite-derived chl *a* for the voyage period (Figure 3c). The highest depth-integrated chl *a* concentrations were encountered at Stations 36 and 39 (>120 mg/m^2), located on the eastern flank of the southern plateau. Integrated chl *a* concentrations >100 mg/m^2 were further observed at stations immediately north of the SB (Figure 2a) including Stations 10, 11, 18, and 27 (noting Station 18 was also located at the ice edge). Stations south of the SB displayed comparatively lower integrated chl *a* concentrations (30–85 mg/m^2), with the exception of Station 21 at the Antarctic shelf break, where chl *a* concentrations were again near 100 mg/m^2. Integrated chl *a* concentrations over the plateau were variable but generally above the low values evident in offshore waters both to the west (Stations 42–44) and northeast (Stations 33–35).

Some differences between in situ and satellite measurements may be expected because integrated chl *a* estimates include deep chlorophyll maxima that are not captured by surface satellite observations. Subsurface chlorophyll maxima were observed at almost half the stations, but a high Pearson correlation coefficient for surface and integrated chl *a* ($r = 0.68$, $n = 35$, $p \ll 0.005$) indicates that they are not a strong confounding factor. Further discrepancies between satellite-measured and in situ chl *a* may arise from spatial and

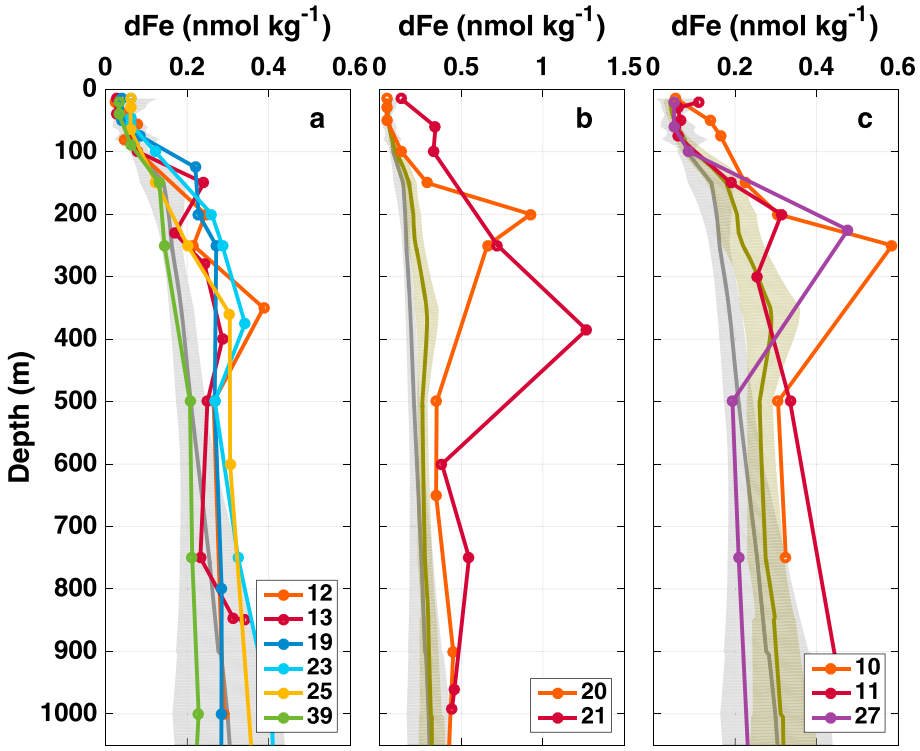

Figure 4. Figures 4a–4c display dFe concentrations (nmol/kg) versus depth for selected regions of interest; values from below the detection limit were replaced with the respective detection limits. (a) dFe for stations below the SB, excepting the two most coastal stations (20 and 21), and overlain on the mean and standard deviation (light gray line and shadow) for 13 stations from the ACC and southern Kerguelen plateau (yellow and red stations in Figure 2a, except Station 27). (b) dFe for coastal Stations 20 and 21, mean and standard deviation for ACC and southern Kerguelen plateau stations as in Figure 4a, and the mean and standard deviation for the stations from Figure 4a displayed in olive; note the different scale on the *x* axis. (c) dFe for Stations 10, 11, and 27, that is, stations with high chl *a* in the PET area; means and standard deviations as in Figure 4b. SB = Southern Boundary; ACC = Antarctic Circumpolar Current; dFe = dissolved iron; PET = Princess Elizabeth Trough.

temporal variations since the satellite data were averaged over a month (18 January to 18 February) and represent spatial averages, while the depth-integrated HPLC data were discretely sampled.

3.3. The dFe Concentrations

The dFe was measured at all stations indicated in Figure 2a. However, only data from stations of interest for the PET and flank blooms are shown in detail in Figures 4 and 5. The complete set of dFe profiles and their respective temperature-salinity diagrams is reported in the supporting information (Figures S3 and S4).

Overall, dFe concentrations encountered on the voyage were very low, especially in surface waters, with almost half the data from the upper 100 m below the respective DL. All dFe profiles showed an increase in concentrations with depth (Figure 4), for the most part staying well below 0.4 nmol/kg to a depth of 1,000 m with some exceptions. The two Antarctic slope stations (Figure 4b) displayed the highest dFe concentrations encountered on the voyage, with a maximum of 1.27 nmol/kg observed at Station 21 near 400-m depth. Both stations had dFe concentrations that were highly elevated compared to all other stations measured (light and dark gray shaded areas in Figure 4b), with this persisting to a depth of 1,000 m.

In the zone south of the SB (Figure 4a), which broadly falls into the main area of the PET bloom in Figure 1, dFe concentrations shallower than 100 m were consistently low ($<$0.1 nmol/kg). Increased variability was observed at depths below 100 m, with dFe concentrations up to 0.4 nmol/kg. Stations in this oceanic region showed elevated dFe relative to stations farther north (light gray shaded area) at depths above ~500 m. The only station for which this was not the case was Station 39, which had low dFe concentrations ($<$0.25 nmol/kg) to a depth of 1,000 m.

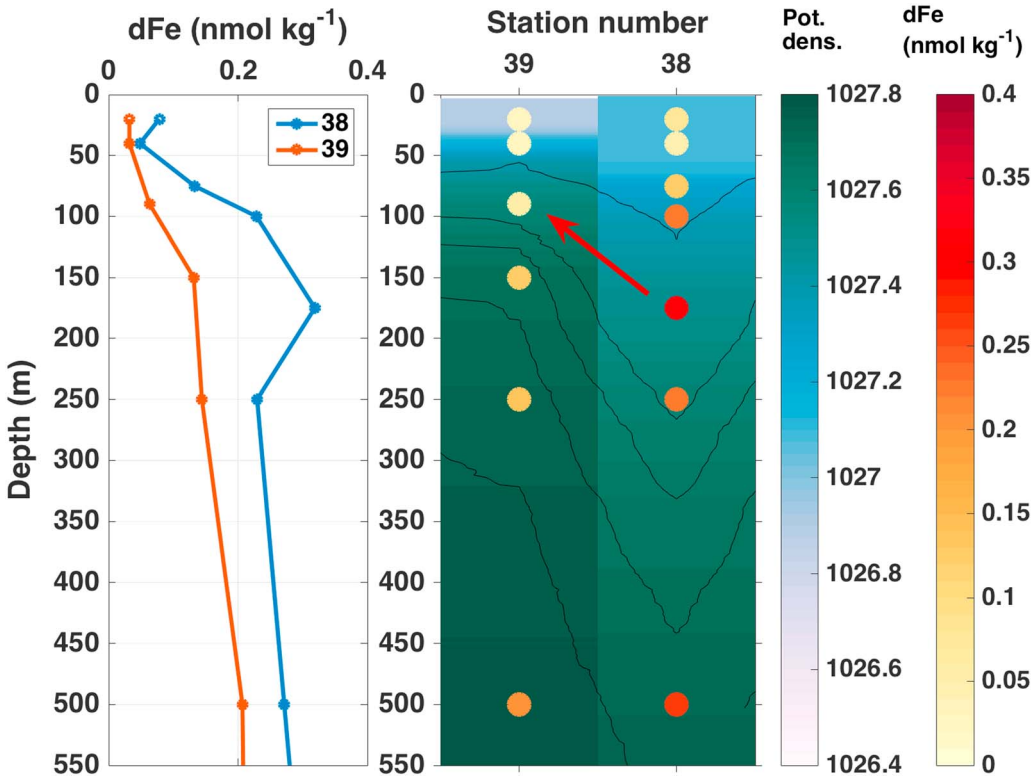

Figure 5. Detail of frontal Stations 38 and 39 at the eastern edge of the southern Kerguelen plateau: Depth profiles of dFe are on the left, and color-coded dFe concentrations (colored circles) overlain on potential density (kg/m^3; background colors) are on the right. Thin black lines in right panel indicate isopycnal surfaces; arrow shows potential upwelling along isopycnals. dFe = dissolved iron.

Figures 4c and 5 display dFe concentrations for key stations where integrated chl *a* was high and which also fall in the two main southern bloom regions of interest: the PET (Stations 10, 11, and 27, Figure 4c) and the eastern flank of the southern Kerguelen plateau (Stations 38 and 39, Figure 5). Stations 18 and 21, which also had high chl *a*, are not included here because they were likely affected by localized iron sources that are not expected to sustain the PET bloom through the season (see section 4.7 for details).

Of these key stations with high chl *a* observations (Figures 4c and 5), only Station 10 showed elevated dFe near the ocean surface. All other stations (Stations 11, 27, and 39) displayed unremarkable and low dFe concentrations between 0 and 100 m. Surface dFe distributions therefore cannot explain the observed high chl *a* distributions. However, dFe in the subsurface (i.e., between 200 and 300 m) was significantly elevated at the high-chl *a* stations in the PET (Figure 4c). This was not the case for Station 39 on the eastern flank of the plateau (Figure 5), which was instead in close proximity (~50 km) to a station with considerably higher dFe concentrations at all depths (Station 38).

3.4. Nitrogen Stable Isotopes

The particulate nitrogen isotopic composition (Figure 6) suggests two distinct regions relative to each other with respect to nitrogen uptake. Negative δ^{15}N (warm colors) were observed over the southern Kerguelen plateau and to the west, while positive δ^{15}N prevailed along the flank east of the plateau and in the PET area. Positive δ^{15}N indicate nitrate uptake, suggesting that new production was occurring in these areas and nitrate uptake was not limited by iron availability (Karsh et al., 2003; Trull et al., 2008, 2015). In contrast, the negative δ^{15}N over the plateau and further to the west suggest nitrogen recycling and ammonia uptake (Trull et al., 2015). We note that the areas where the δ^{15}N signature indicates new production are colocated with the persistent blooms around the southern Kerguelen plateau (Figure 1).

These results indicate that during the *K* axis voyage, the bloom areas around the southern Kerguelen plateau (i.e., the locations of the PET and eastern flank blooms) were thriving with new primary production (Figure 6).

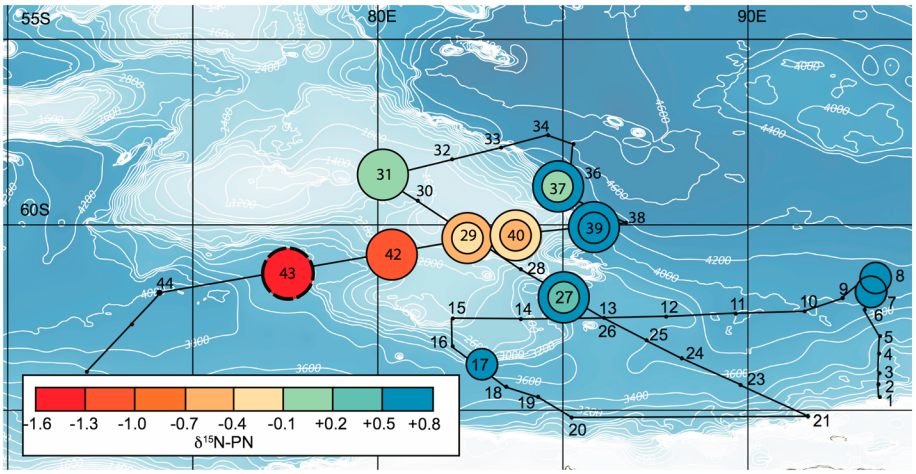

Figure 6. Particulate nitrogen isotopic composition of two size fractions of suspended particles sampled underway (from 5-m depth). Smaller cells (1.2 to 210 μm) are represented by smaller circles, and larger cells (210 to 1000-μm) are represented by the larger circles. Station 43 sample (dashed outline) was from 50 m. Stations with cooler colors are indicative of nitrate uptake and new production. Lower δ^{15}N values (warmer colors) suggest ammonia recycling. Cruise track and station numbers are in black, and bathymetric contours are in white.

New production is consistent with recent and/or regular dFe supply to these areas, as nitrate and silicate in surface waters were not limiting anywhere during the *K* axis voyage, with the lowest measured silicate concentrations around 13 μmol/L and the lowest nitrate concentrations around 17 μmol/L (data not shown). This interpretation is further supported by the direct visual observation under microscopy of diatoms of the genera *Chaetoceros*, *Rhizosolenia*, *Proboscia*, and *Corethron* at the high-chl *a* stations (Stations 10, 11, 27, and 39), while the number of dinoflagellates was very low (unpublished data, but see examples of microscopy images in Figure S5). Although this evidence is indirect, diatoms of the genera *Chaetoceros* and *Corethron* are known to respond strongly to Fe fertilization (de Baar et al., 2005). Furthermore, Station 39 had *Phaeocystis* in the colonial form, which has a higher Fe requirement than the solitary form (Bender et al., 2018; Garcia et al., 2009). These observations thus point to recent and potentially sustained dFe supply at these stations.

4. Discussion

We explore different dFe supply mechanisms and attempt to link them to the observed chl *a* distributions, exploring hypotheses put forward in previous publications:

1. The PET bloom receives dFe and phytoplankton that are advected off the Antarctic shelf by a strong northerly surface flow near 85°E (Rintoul et al., 2008).
2. The flank bloom is supplied with dFe by vertical motion, resulting from the main current flow interacting with topography (Sokolov & Rintoul, 2007).

Building on our observations and inferences, we show that the persistence of the southern Kerguelen phytoplankton blooms is best explained by vertical dFe supply resulting from frontal processes associated with the sACCf and SB, with the subsurface dFe likely to be mainly sourced from sediments of the Antarctic continental shelf and slope.

In what follows we treat the high-chl *a* stations north of the SB (i.e., Stations 10, 11, and 27) as representative of the greater PET bloom as identified in the chl *a* climatologies (Figure 1), while we consider Station 39 as representative for the flank bloom. We first examine the PET bloom and its dFe supply, followed by an investigation of the flank bloom.

4.1. Evaluating the Advection Hypothesis

Rintoul et al. (2008) investigated the annual formation of a sea ice tongue over the PET near 85°E and found that the surface flow here is directed away from the Antarctic shelf in a northerly direction as a consequence of the topographic steering around the southern Kerguelen plateau. They hypothesized that this northward

advection could also transport high concentrations of micronutrients (including Fe) and phytoplankton from the productive shelf waters to the PET, causing the annual bloom in the area (Rintoul et al., 2008). Our observations indicate that dFe (Figure 4a) and in situ chl *a* concentrations (Figure 2b) over the main area of the PET were moderate during the *K* axis voyage compared to the high-chl *a* stations (Stations 10, 11, and 27) just north of the SB (Figures 2b and 3a). Thus, the area where offshore advection of waters from the shelf is expected to be highest (around 85°E, see also Figure 2a) had lower chl *a* concentrations than the region to the north. This general pattern is also observed in the January chl *a* climatology for the region, showing an area of relatively lower chl *a* concentrations over the southern PET that is contrasted by higher chl *a* concentrations further north (Figure 1b). We therefore conclude that lateral advection of surface waters from the shelf is unlikely to be responsible for the observed PET bloom.

4.2. Formulating a New Hypothesis

The question then remains: What does sustain the PET bloom? Examination of Figure 4c reveals that surface dFe concentrations at the high-chl *a* stations (10, 11, and 27) did not show a coherent pattern for these stations, with only Station 10 displaying elevated dFe in the upper 100 m. However, all three stations showed elevated dFe concentrations in the subsurface, and the high dFe in this depth range was well above concentrations observed elsewhere on the voyage, excepting the two coastal stations (Figure 4b). A similar pattern of enhanced dFe at depth was also observed over the northern Kerguelen plateau during the first KEOPS campaign, where natural iron fertilization from depth was inferred to result from deep winter mixing and elevated vertical diffusivity due to internal wave activity, sustaining the persistent bloom over the plateau (Blain et al., 2008; Park et al., 2008). The range of deep dFe concentrations observed by Blain et al. (2008) was similar to ours (maximum dFe ~0.6 nM). However, the source of the deep dFe enhancement over the shallow northern Kerguelen plateau was most likely the underlying sediment, which cannot be the dFe source over the PET, where water depths are $>$3,000 m.

We shall return to the question of the deep dFe source, but we first explore the possible links between a subsurface dFe enhancement and the biota in the surface layer. First, we consider the concept of the ferricline, and second, different mechanisms for supplying dFe from depth to the surface ocean will be investigated.

The ferricline, which is the depth where dFe concentrations increase *considerably* relative to surface concentrations, can be defined in many different ways. One method is to take the depth of the maximum dFe gradient as the ferricline (Tagliabue et al., 2014). Other definitions, such as the depth where a certain threshold concentration is crossed, may be more useful in terms of defining the depth from which Fe supply could come to fuel euphotic zone productivity. We applied both definitions to the *K* axis data (Figure 7 and Table 1), applying a conservative dFe threshold (0.15 nmol/kg) based on the modeling study by Mongin et al. (2009), which found dFe concentrations of 0.03–0.13 nmol/L at the edges of the northern Kerguelen bloom. Both definitions yield similar depths for the ferricline in all regions except the ACC, where dFe concentrations were extremely low and the threshold ferricline was thus considerably deeper than the gradient ferricline (Figure 7d). For all other regions, the ferricline depth was 100–150 m, which is slightly shallower than the 150- to 200-m ferricline observed over the northern Kerguelen plateau (Blain et al., 2008) and the ~200-m ferricline downstream of the northern Kerguelen plateau (Quéroué et al., 2015). Notably, it is considerably shallower than the mean Southern Ocean ferricline of 333 m estimated by Tagliabue et al. (2014) based on 140 dFe profiles from the open ocean.

While the ferricline depth did not vary greatly between the oceanic zones sampled on *K* axis (with the exception of the ACC threshold ferricline mentioned above), the dFe gradients and concentrations at the ferricline depth showed considerable variability (Table 1). The high-chl *a* stations over the PET (Stations 10, 11, and 27) stood out as having the consistently highest dFe concentrations and gradients compared to the other regions (Table 1), supporting the concept that a vertical supply mechanism would be most effective at bringing dFe into the surface layer at these stations. We thus put forward the hypothesis that the observed elevated dFe concentrations and gradients in the subsurface are related to enhanced chl *a* concentrations near the surface. The question then becomes, How does the deep dFe reach the surface layer of the ocean?

4.3. Vertical dFe Supply to the PET Bloom

Vertical processes that could bring subsurface dFe to surface waters include vertical eddy diffusivity, deep mixing, and upwelling. The coarse vertical resolution of the available CTD data (2 m) precludes confident

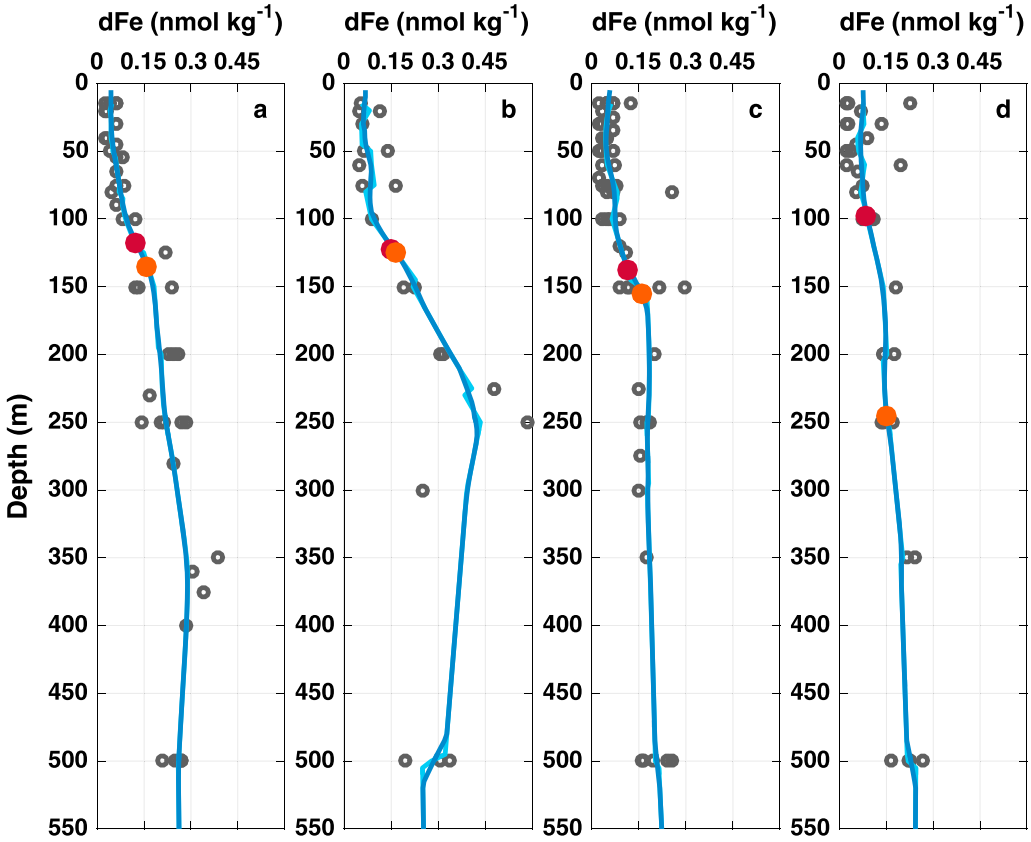

Figure 7. Investigation into the depth of the ferricline for different oceanic zones: (a) Data from stations south of the SB, except Stations 20 and 21; (b) from Stations 10, 11, and 27 (i.e., the high-chl *a stations of interest*); (c) from stations north of the sACCf (yellow in Figure 2a, Station 27 not included); (d) from ACC stations (red in Figure 2a). Gray dots are measured dFe data, light blue lines represent average dFe for the respective panel, and dark blue lines are the smoothed averages. The latter were used for two different estimates of the ferricline depth: The maximum dFe gradient in the top 500 m (dark red) and the depth threshold where dFe $>$ 0.15 nmol/kg (orange). SB = Southern Boundary; sACCf = south Antarctic Circumpolar Current front; ACC = Antarctic Circumpolar Current; dFe = dissolved iron.

estimates of vertical eddy diffusivity, but given the steep dFe gradient identified above, even invariant vertical diffusivity in the region would produce enhanced dFe input at the PET stations. Vertical diffusivity can increase at fronts and due to the interaction of baroclinic tides with steep bathymetric features, with the latter thought to supply dFe from depth to the sustained phytoplankton bloom over the northern Kerguelen plateau (Blain et al., 2008; Park et al., 2008). There is no reason to expect this tidal influence over the greater PET as it is topographically quite flat. However, given that the PET stations are all located near major ACC fronts (Figure 2), enhanced vertical diffusivity associated with steep frontal density gradients may add to the vertical dFe flux at these stations.

Table 1
Ferricline Details for Different Oceanic Zones During K Axis

Oceanic zone (corresponding to panels in Figure 7) Units	dFe conc. at the *gradient ferricline* nmol/kg	dFe gradient at the *gradient ferricline* nmol/m^4	dFe gradient at the *threshold ferricline* nmol/m^4	Depth range *gradient ferricline* m	Depth range *threshold ferricline* m
Below SB, excluding Stations 20 and 21 (Figure 7a)	0.13	2.0	1.8	~120	~130
Stations 10, 11, and 27 (Figure 7b)	0.17	3.2	3.2	~120–130	~130
North of sACCf (Figure 7c)	0.13	2.4	1.8	~140	~150
ACC (Figure 7d)	0.09	1.0	0.6	~100	~240–250

Note. SB = Southern Boundary; sACCf = south Antarctic Circumpolar Current front; ACC = Antarctic Circumpolar Current; dFe = dissolved iron.

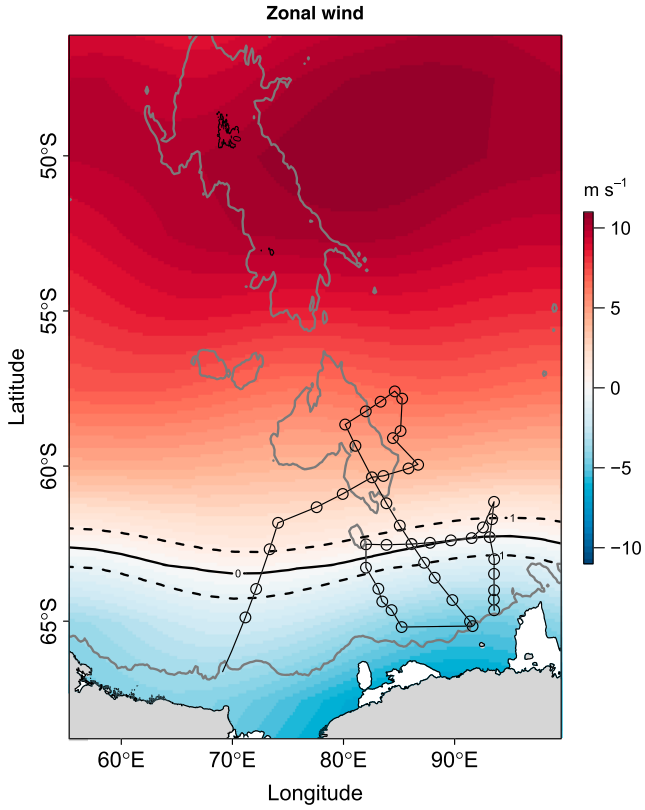

Figure 8. Mean zonal summer wind field at 10 m above the surface from a 10-year climatology of monthly NCEP/DOE wind reanalysis (Raymond, 2014). The latitude at which the shift from eastward to westward winds occurs, that is, the latitude of the Antarctic Divergence, is indicated by the solid black contour (mean zonal wind = 0); dashed lines are contours for zonal wind speeds of 1 m/s. Cruise track, station locations, and 2,000-m bathymetry contour (gray) are also indicated. NCEP = National Centers for Environmental Prediction; DOE = Department of Energy.

Deep winter mixing, which appears to dominate dFe supply in the Southern Ocean in general by generating a strong wintertime iron pulse (Tagliabue et al., 2014), is an unlikely candidate to play an important role in the seasonally ice-covered PET, where winter mixing depths were between 100 and 150 m (based on the winter water layer estimated using isotherms from the CTD data). The exceptions were at the coastal Stations 20–22 (and the associated Station 26), where the winter water extended up to 400 m in the Antarctic Slope Current. The relatively shallow winter mixing estimates are consistent with observations for seasonally sea ice covered areas elsewhere around Antarctica, where the under ice mixing depth was estimated at only ~120 m (Pellichero et al., 2017). Indeed, melting of the ice in spring increases stratification of the water column, reducing wind-induced mixing (Buesseler et al., 2003; Smith & Nelson, 1985; Vancoppenolle et al., 2013). We thus conclude that neither deep winter mixing nor enhanced vertical diffusivity from internal tides is likely to constitute a sustained dFe source throughout the PET.

The PET stations' proximity to the sACCf and SB may also have implications for upwelling. These fronts are thought to be the main conduits for the meridional exchange of salt and heat in the area (Heywood et al., 1999), and the SB is an area of potential upwelling. South of the ACC is an important upwelling region termed the Antarctic Divergence, resulting from northward Ekman transport in the ACC (driven by westerly winds) and a southward Ekman transport closer to the Antarctic coast (driven by easterly winds, Figure 8). This atmospherically determined feature acts to draw upper circumpolar deep water (UCDW) into the surface waters, hence may be colocated with the SB (Bindoff et al., 2000). Although the precise position of zero mean zonal flow is difficult to determine, the stations where elevated chl *a* was observed in the PET (i.e., Stations 10, 11, and 27) notably all fall into the band of minimum mean zonal winds in summer (Figure 8) that may be indicative of the location of the Antarctic Divergence climatologically.

We thus propose that upwelling along the meandering SB combined with a shallow, steep ferricline could supply dFe to surface waters and explain the high chl *a* concentrations observed at Stations 10, 11, and 27. This upwelling associated with the Antarctic Divergence is particular to the PET area and is not occurring around the northern Kerguelen plateau. We note that the ferricline was relatively shallow for all waters south of the SB (Figure 7a), and dFe concentrations in the 150- to 600-m range here were also moderately elevated (Figure 4a). Upwelling anywhere over the PET would therefore readily supply some dFe to the photic zone, and this may explain the moderate chl *a* observed here. In comparison, the bloom downstream of the northern Kerguelen plateau is believed to chiefly receive its dFe supply via horizontal transport in the surface (Bowie et al., 2015; D'Ovidio et al., 2015). The unstated implication is that during the growing season, this dFe source weakens as phytoplankton take up the iron where it first enters surface waters, that is, over the northern Kerguelen plateau. The northern and southern blooms are thus supplied by fundamentally different (i.e., horizontal versus vertical) mechanisms, which could explain the difference in longevity between the two blooms.

4.4. A Role for Retention?

Another important difference between the northern and southern blooms is the magnitude of the horizontal velocity in the respective areas (Figure S6). In the PET south of the SB, currents are generally low, <3 cm/s (Bestley et al., 2018; see also geostrophic currents in Figure 2a). Quiescent flow and recirculation may contribute to high retention of phytoplankton and iron that is advected into this region. Such retention would make Fe recycling by the community very effective, contributing to the longevity of the bloom. For example, Boyd et al. (2015) observed very high Fe recycling efficiency (supplying up to 90% of Fe demand) in low-iron waters east of New Zealand, emphasizing that Fe recycling can be an important component of the Fe supply

in iron-limited regions. In comparison, the area of the northern offshore bloom is affected by the strong eastward advection of the ACC currents (Figure S6). Here strong mesoscale activity is the likely mechanism moderating otherwise fast dispersal of phytoplankton and any recycled iron (Cotté et al., 2015; D'Ovidio et al., 2013).

4.5. Source of the Subsurface dFe Enhancement

Here we return to the question of the deep dFe source. The high observed dFe concentrations of up to 0.6 nmol/kg at Stations 10 and 27 (Figure 4c) are outside the range of concentrations observed in UCDW south of the Polar Front (i.e., away from point sources), which usually does not show concentrations above ~0.4 nmol/L (Klunder et al., 2011; Quéroué et al., 2015). UCDW is therefore an unlikely source for the high observed dFe concentrations. Shallow remineralization, transport of subsurface dFe from the Antarctic shelf, and sea ice melt are all potential contributors to the dFe enhancement and will be examined in more detail below.

Given the general longevity of the phytoplankton bloom in the area (Figure 1), efficient remineralization of sinking biomass from earlier bloom stages is a conceivable dFe source to subsurface waters at Stations 10, 11, and 27. Apparent oxygen utilization in the 150- to 300-m depth layer was slightly elevated at these stations relative to deeper depths and compared to stations from south of the SB (data not shown), with Station 27 showing the strongest apparent oxygen utilization signature, followed by Stations 10 and 11. Remineralization of organic matter, with a concomitant release of dFe, is thus a feasible explanation for at least part of the observed subsurface dFe enhancements at these stations.

However, advection of subsurface dFe from the Antarctic shelf is also a possibility, suggested in part by the clear similarity evident in the profile shapes in Figures 4b and 4c. Indeed, the 400-m dFe maximum at Station 21 coincided with slightly increased turbidity (data not shown), suggesting the presence of resuspended sediments. Stations 10, 11, and 27 lie within the 95% prediction bounds of a power model relating column-integrated dFe concentrations to distance from the shelf (i.e., distance from nearest area of seafloor $\leq$500-m deep) for waters south of the SB (Figure 9a). Including the three stations in a Pearson correlation between integrated dFe and distance from shelf yields $r = -0.73$ and $p = 0.01$; excluding the three stations yields $r = -0.76$ and $p = 0.03$. These results indicate that Stations 10, 11, and 27 fall along the same dilution/mixing gradient for dFe with increasing distance from the shelf as the other PET stations south of the SB. Power relationships between integrated dFe concentrations and distance from the coast have been observed in other sectors of the Southern Ocean where continental margins constitute an important dFe source (e.g., de Jong et al., 2012; de Jong et al., 2015), and the contribution of shallow sediments to strong vertical dFe gradients in waters proximate to the Antarctic continent was recently highlighted by Sherrell et al. (2018).

Distance from the shelf and time since ice melt varies colinearly ($r = 0.79$); hence, the correlation of dFe with time since ice melt (Figure 9b) is also strong. It is thus difficult to differentiate between the two based on correlations. But ice melt is not expected to add dFe at depths below the mixed layer (Schallenberg et al., 2016), and shelf sediments are a much more likely candidate for adding dFe to subsurface waters (de Jong et al., 2012; Marsay et al., 2014; Schallenberg et al., 2016). The negative correlation of dFe with potential temperature and the positive correlation with oxygen (Figures 9c and 9d) further illustrate the shelf linkage, shelf waters being cold and well oxygenated (Bestley et al., 2018; Bindoff et al., 2000). The sea ice, on the other hand, had retreated $>$40 days before Stations 10, 11, and 27 were occupied (Figure 9b), and no subsurface enhancement of dFe was found at other stations with similar sea ice exposure either north or south of the SB. Hence, the Antarctic shelf is a more likely source of the elevated subsurface dFe at Stations 10, 11, and 27 than is sea ice melt.

Along the Antarctic margin, some component of the westward flowing Antarctic Slope Front diverts offshore and feeds the SB flow, forming the western edge of the cyclonic gyre in the Australia-Antarctic Basin (Bindoff et al., 2000; McCartney & Donohue, 2007; Park et al., 2009). The *K* axis survey did sample a distinctive mesoscale feature in the upper 300 m with anomalously cold, fresh, oxygenated properties very similar to those observed at the Antarctic slope stations, some 300 km farther north (Station 26 at 62.5°S, 86°E; Figure S7; no dFe data available). This feature was not evident during the first pass at that location (Station 13), so the CTD data set cannot show conclusively whether the eddy of Antarctic Slope Front water was an

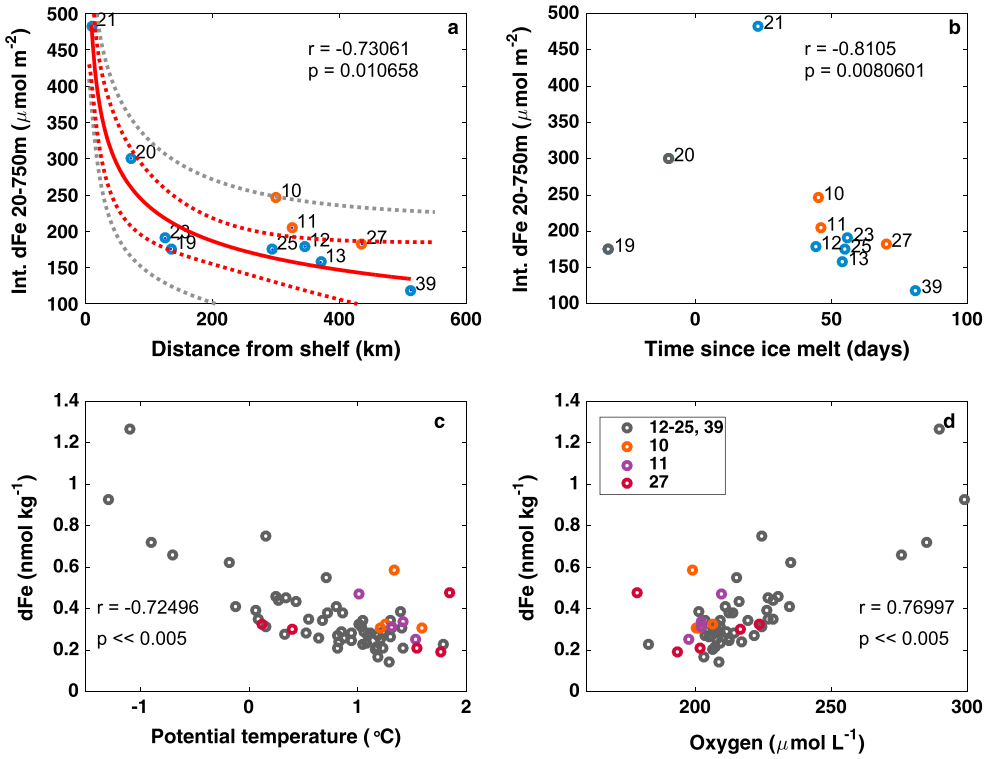

Figure 9. Figures 9a and 9b show integrated dFe between 20 and 750 m versus distance from shelf (a) and time since ice melt (b) for stations from south of the southern boundary, including Station 39, and also for the high-chl *a* Stations 10, 11, and 27 (highlighted in orange). A best fit power model of the form $y = a^*x^b + c$ (red) was calculated for stations from south of the SB only (blue circles). Shown are also the 95% prediction bounds for the fitted curve (red dashed) as well as the 95% prediction bounds that account for the uncertainty of predicting the fitted curve plus the random variation in the new observation (gray dashed). Figures 9c and 9d show measured dFe values versus potential temperature and oxygen concentration for depths >150 m for the same stations ($n = 66$). Pearson correlation coefficients, r, and associated p values are displayed in each panel; note that in Figure 9b, Stations 19 and 20 were excluded from the correlation. Time since ice melt is from Bestley et al. (2018), and distance from shelf is from the catalog of Australian Antarctic and Subantarctic metadata (http://share.biodiversity.aq/GIS/antarctic/netcdf/). SB = Southern Boundary; dFe = dissolved iron.

isolated feature or part of a more continuous flow. However, this observation is consistent with the mesoscale eddies repeatedly observed by Aoki et al. (2007) farther east near 140°E. Such cyclonic eddies appear to be generated by instabilities near the continental slope and are subsequently observed along the northern edge of the Antarctic Divergence (Aoki et al., 2007; Wakatsuchi et al., 1994). In this study, daily contours of sea surface height are consistent with northward transport along 85°E, as found by Rintoul et al. (2008), and subsequent meandering in an easterly direction in the PET (Bestley et al., 2018, their Figure 6). A series of dynamic cold- and warm-core eddy features was also evident in the vicinity of the sACCf and the SB during the survey period (Bestley et al., 2018, their supporting information). It is thus possible that instabilities forming near the continental slope, carrying dFe-rich waters in the subsurface, may then travel along the SB. Upwelling processes associated with the Antarctic Divergence, and potentially with mesoscale eddy processes, may lift the elevated subsurface dFe (i.e., at Stations 10, 11, and 27) into surface waters.

4.6. Iron Supply to the Flank Bloom

An eastern flank bloom is apparent in the chl *a* climatology (Figure 1) and is coincident with the area where high integrated chl *a* was observed during the *K* axis voyage (Stations 39 and 36). However, the dFe profile for Station 39 (no dFe data available for Station 36 and neighboring stations) shows much lower dFe at depth than was observed for the PET bloom stations (compare Figures 4c and 5). This suggests that direct upwelling will be less effective in supplying dFe here than is the case at the PET stations. Nevertheless, the location of Station 39 is in a region where the ACC interacts with topography, creating very strong flow with steeply

sloping isopycnals (Figure 5). This should lead to high vorticity and strain rates, and as a consequence potentially to strong vertical transport along isopycnals by submesoscale turbulence (Mahadevan, 2016). Given the elevated dFe concentrations found subsurface across the sACCf (Station 38, Figure 5), such transport along steep isopycnals could supply dFe from depth into the mixed layer. The elevated dFe at Station 38 was associated with warmer waters transported from the north by the FTC (Bestley et al., 2018). However, given only one station from this offshore flow was sampled for trace elements (Figure 2a), it is difficult to speculate further about the source of this dFe.

Upwelling along the flank of the southern Kerguelen plateau is also generally consistent with the findings by Sokolov and Rintoul (2007). Investigating the connection between deep bathymetric features (including the southern Kerguelen plateau) and elevated chl *a* in their vicinity, these authors found that the bottom pressure torque resulting from the main flow interacting with topography produces persistent upwelling around the edges of the topography. A persistent upwelling mechanism in this area would be consistent with the climatology showing enhanced chl *a* along the southeastern flank of the plateau throughout the growing season (Figure 1).

The bathymetric steering of the sACCf around the southern Kerguelen plateau may contribute to the flank bloom in additional ways. For example, the strong retroflection of this feature (see shape of the sACCf east of the southern Kerguelen plateau in Figure 2a) may serve to enhance retention of phytoplankton within a tight band along the eastern flank of the plateau. Such a large-scale feature is absent in the strong jets found to the east of the northern Kerguelen plateau, which is more likely to disperse phytoplankton than to retain them in a confined area. In addition, some component of the phytoplankton biomass from the PET may also be advected along the eastern flank of the plateau by the sACCf, further contributing to the accumulation of biomass in the area.

4.7. Localized dFe Input

There were two additional high-chl *a* stations (Stations 18 and 21) that were separated from the analysis above because their dFe supply was considered likely to be related to localized sources such as sea ice melt and direct sedimentary input from the shelf break, respectively. While sedimentary dFe input may indirectly supply dFe to the PET bloom, as outlined above, sea ice melt is unlikely to play a role in sustaining the bloom.

Station 18 was located at the immediate ice edge and thus is a strong candidate for an ice edge bloom, with recent ice melt supported by the presence of cold, fresh water near the surface (Bestley et al., 2018). Melting sea ice has been observed to support increased phytoplankton growth, presumably due to increased light levels in a stabilized water column and also due to the release of dFe (Croot et al., 2004; Lannuzel et al., 2016; Sedwick & DiTullio, 1997; Smith & Nelson, 1985). However, ice edge blooms tend to be relatively short lived (Buesseler et al., 2003), so melting sea ice is not a likely candidate supporting the sustained PET bloom. Indeed, the sea ice over the main area of the PET had retreated $>$40 days before stations were occupied (Figure 9b), and relatively moderate chl *a* concentrations (i.e., not bloom conditions) were observed here during the voyage (e.g., Stations 12, 13, and 23–25; Figure 2b). However, sea ice melt earlier in the season is likely to contribute to the initial bloom as observed in the southern sector of the PET in the December climatology (Figure 1).

4.8. Suggestions for Future Sampling Design

In order to confirm our hypotheses regarding dFe supply to the PET, a future study should aim for a sampling design that includes a long transect along 85°E from the shelf to at least 60°S, in order to traverse both the SB and the sACCf. This should be matched with a paired transect immediately to the east. To better resolve dFe sources from the north, we would recommend a grid with east-west transects, covering the eastern flank of the southern Kerguelen plateau and traversing past the sACCf retroflection well into the warm northerly flow. Analysis of iron isotopes and measurement of Fe pools in suspended particles might help to further constrain the source of the dFe, and estimates of vertical velocity, for example, from a Lowered Acoustic Doppler Current Profiler, would be highly desirable as well.

5. Summary and Conclusions

We investigated the dFe sources around the southern Kerguelen plateau with a particular view to explaining the chl *a* climatologies in the region, which show sustained phytoplankton blooms over the PET and on the

eastern flank of the plateau. Our analysis indicates that the sustained blooms are supplied by vertical dFe input, as was also observed for the sustained bloom over the northern Kerguelen plateau (Blain et al., 2008). The vertical supply mechanisms and dFe sources differ between these regions as follows:

1. The PET bloom is supplied by subsurface dFe most likely delivered by subsurface advection from the Antarctic shelf sediments, supplemented by remineralization of biomass from earlier bloom stages. Upwelling of this dFe is expected to mainly result from Ekman pumping associated with the Antarctic Divergence, with an additional potential role of mesoscale eddy processes.
2. The eastern flank bloom likely receives dFe from the subsurface via isopycnal upwelling, by mesoscale and submesoscale turbulence, along the strong jet resulting from the interaction of the sACCf with the southern Kerguelen plateau.
3. Over the northern Kerguelen plateau, sedimentary dFe reaches surface waters as a consequence of deep winter mixing and enhanced vertical diffusivity resulting from internal tides (Blain et al., 2008; Park et al., 2008).

In contrast, the large phytoplankton bloom downstream of the northern Kerguelen plateau is not sustained throughout the season but *blooms and busts* (Figure 1). This bloom is believed to receive most of its dFe supply from lateral advection of surface waters, with the horizontal advection term 4–5 times larger than the vertical term (Bowie et al., 2015). It thus appears that sustained vertical dFe supply is conducive to sustained phytoplankton blooms, while lateral dFe supply in surface waters is more likely to support a spring bloom that subsequently declines (Figure 1). We suspect that the horizontal dFe supply to the phytoplankton bloom downstream of the northern Kerguelen plateau is drastically reduced in summer due to primary productivity over the plateau itself, taking up the vertically supplied dFe. This opens the intriguing possibility that the key to the sustained PET bloom is not only the vertical transport particular to the area but also subsurface (as opposed to surface) advection of dFe from the shelf. Similarly, horizontal advection (i.e., via the Fawn Trough) may also play a role in supplying subsurface dFe to the flank bloom. Subsurface horizontal advection is thus expected to play an important role in dFe supply in the region, but only when combined with sustained vertical transport into the photic zone can this dFe source support persistent phytoplankton growth in the surface layer of the ocean.

Acknowledgments
The authors would like to thank two anonymous reviewers for their thoughtful, diligent, and constructive comments on this manuscript. We thank the master and crew of the RV *Aurora Australis* and the Science Technical Support Team of the Australian Antarctic Division (AAD) for their considerable efforts to make this work happen. Furthermore, we are grateful to the chief scientist, Andrew Constable, and to the voyage leader, Lloyd Symons. We also thank Imojen Pearce (AAD) for HPLC analyses and Barbora Gallagher for running the nitrogen isotope analyses at ANSTO. Andrew Stewart of UCLA provided data from a high-resolution global ocean model that enhanced our understanding of the physical processes around the southern Kerguelen plateau. The University of Otago enabled this work by graciously lending us their trace metal container and rosette—many thanks! We would also like to express our gratitude to Kerrie Swadling for sharing the isotope data, which was supported by ANSTO grant 10043. Finally, we thank Steve Rintoul for fruitful discussions about fronts, currents, and upwelling mechanisms. This study is supported by the Australian Government through (i) Australian Antarctic Science projects (Kerguelen Axis project AAS-4344), (ii) the Cooperative Research Centres Programme through the Antarctic Climate and Ecosystems Cooperative Research Centre (ACE CRC), and (iii) the Antarctic Gateway Partnership special research initiative through the Australian Research Council (ARC). Access to ICP-MS instrumentation was supported through ARC LIEF funds (LE0989539). C. S. is supported by a Canadian National Sciences and Engineering Research Council postdoctoral fellowship (NSERC-PDF), A. K. was supported by an Australian Research Council Discovery Early Career Researcher Award (DE140100076). A. R. B. was supported by the Australian Research Council Discovery (DP150100345) and Future Fellowships (FT130100037) programs. K. W. was supported by Australian Antarctic Science grant 4344 at the Australian Antarctic Division. The IAEA is grateful to the Government of the Principality of Monaco for the support provided to its Environment Laboratories. We acknowledge the NCEP_Reanalysis 2 data provided by the NOAA/OAR/ESRL PSD, Boulder, Colorado, USA, from their website at http://www.esrl.noaa.gov/psd/. All CTD (doi:10.4225/15/5ade-c86550a1a), dFe (doi:10.4225/15/5a77d6bd5975e), and isotope data presented in this manuscript are available

References

Aoki, S., Fukai, D., Hirawake, T., Ushio, S., Rintoul, S. R., Hasumoto, H., et al. (2007). A series of cyclonic eddies in the Antarctic Divergence off Adelie coast. *Journal of Geophysical Research*, *112*, C05019. https://doi.org/10.1029/2006JC003712

Aoki, S., Fujii, N., Ushio, S., Yoshikawa, Y., Watanabe, S., Mizuta, G., et al. (2008). Deep western boundary current and southern frontal systems of the Antarctic Circumpolar Current southeast of the Kerguelen Plateau. *Journal of Geophysical Research*, *113*, C08038. https://doi.org/10.1029/2007JC004627

de Baar, H., Boyd, P. W., Coale, K. H., Landry, M. R., Tsuda, A., Assmy, P., et al. (2005). Synthesis of iron fertilization experiments: From the Iron Age in the Age of Enlightenment. *Journal of Geophysical Research*, *110*, C09S16. https://doi.org/10.1029/2004JC002601

de Baar, H., de Jong, J., Bakker, D., Löscher, B., Veth, C., Bathmann, U., & Smetacek, V. (1995). Importance of iron for plankton blooms and carbon dioxide drawdown in the Southern Ocean. *Nature*, *373*(6513), 412–415. https://doi.org/10.1038/373412a0

Bender, S. J., Moran, D. M., McIlvin, M. R., Zheng, H., McCrow, J. P., Badger, J., et al. (2018). Iron triggers colony formation in *Phaeocystis antarctica*: Connecting molecular mechanisms with iron biogeochemistry. *Biogeosciences Discussions*, 1–52. https://doi.org/10.5194/bg-2017-558

Bestley, S., van Wijk, E., Rosenberg, M., Eriksen, R., Corney, S., Tattersall, K., & Rintoul, S. (2018). Ocean circulation and frontal structure near the southern Kerguelen plateau: The physical context for the Kerguelen axis ecosystem study. Deep Sea Research II SI on Kerguelen Axis Food Webs. https://doi.org/10.1016/j.dsr2.2018.07.013

Bindoff, N., Rosenberg, M., & Warner, M. (2000). On the circulation and water masses over the Antarctic continental slope and rise between 80 and 150°E. *Deep-Sea Research Part II: Topical Studies in Oceanography*, *47*(12-13), 2299–2326. https://doi.org/10.1016/S0967-0645(00)00038-2

Blain, S., Sarthou, G., & Laan, P. (2008). Distribution of dissolved iron during the natural iron-fertilization experiment KEOPS (Kerguelen plateau, Southern Ocean). *Deep-Sea Research Part II: Topical Studies in Oceanography*, *55*(5-7), 594–605. https://doi.org/10.1016/j.dsr2.2007.12.028

Bowie, A. R., Lannuzel, D., Remenyi, T. A., Wagener, T., Lam, P. J., Boyd, P. W., et al. (2009). Biogeochemical iron budgets of the Southern Ocean south of Australia: Decoupling of iron and nutrient cycles in the subantarctic zone by the summertime supply. *Global Biogeochemical Cycles*, *23*, GB4034. https://doi.org/10.1029/2009GB003500

Bowie, A. R., van der Merwe, P., Trull, T. W., Quéroué, F., Fourquez, M., Planchon, F., et al. (2015). Iron budgets for three distinct biogeochemical sites around the Kerguelen plateau (Southern Ocean) during the natural fertilization experiment KEOPS-2. *Biogeosciences*, *12*(14), 4421–4445. https://doi.org/10.5194/bg-12-4421-2015

Boyd, P. W., Jickells, T., Law, C. S., Blain, S., Boyle, E. A., Buesseler, K. O., et al. (2007). Mesoscale iron enrichment experiments 1993–2005: Synthesis and future directions. *Science*, *315*(5812), 612–617. https://doi.org/10.1126/science.1131669

Boyd, P. W., Strzepek, R. F., Ellwood, M. J., Hutchins, D. A., Nodder, S. D., Twining, B. S., & Wilhelm, S. W. (2015). Why are biotic iron pools uniform across high- and low-iron pelagic ecosystems? *Global Biogeochemical Cycles*, *29*, 1028–1043. https://doi.org/10.1002/2014GB005014

from the Australian Antarctic Data Centre: https://data.aad.gov.au.

Buesseler, K. O., Barber, R. T., Dickson, M.-L., Hiscock, M., Moore, J. K., & Sambrotto, R. (2003). The effect of marginal ice-edge dynamics on production and export in the Southern Ocean along 170°W. *Deep-Sea Research Part II: Topical Studies in Oceanography*, *50*(3-4), 579–603. https://doi.org/10.1016/S0967-0645(02)00585-4

Cotté, C., D'Ovidio, F., Dragon, A.-C., Guinet, C., & Lévy, M. (2015). Flexible preference of southern elephant seals for distinct mesoscale features within the Antarctic Circumpolar Current. *Progress in Oceanography*, *131*, 46–58. https://doi.org/10.1016/j.pocean.2014.11.011

Croot, P. L., Andersson, K., Öztürk, M., & Turner, D. R. (2004). The distribution and speciation of iron along 6°E in the Southern Ocean. *Deep-Sea Research Part II: Topical Studies in Oceanography*, *51*(22-24), 2857–2879. https://doi.org/10.1016/j.dsr2.2003.10.012

Cutter, G., Andersson, P., Codispoti, L., Croot, P., Francois, R., Lohan, M., et al. (2010). Sampling and sample-handling protocols for GEOTRACES cruises. http://epic.awi.de/34484/

D'Ovidio, F., De Monte, S., Della Penna, A., Cotté, C., & Guinet, C. (2013). Ecological implications of eddy retention in the open ocean: A Lagrangian approach. *Journal of Physics A: Mathematical and Theoretical*, *46*(25), 254023. https://doi.org/10.1088/1751-8113/46/25/254023

D'Ovidio, F., Della Penna, A., Trull, T. W., Nencioli, F., Pujol, M.-I., Rio, M.-H., et al. (2015). The biogeochemical structuring role of horizontal stirring: Lagrangian perspectives on iron delivery downstream of the Kerguelen plateau. *Biogeosciences*, *12*(19), 5567–5581. https://doi.org/10.5194/bg-12-5567-2015

Garcia, N. S., Sedwick, P. N., & DiTullio, G. R. (2009). Influence of irradiance and iron on the growth of colonial *Phaeocystis antarctica*: Implications for seasonal bloom dynamics in the Ross Sea, Antarctica. *Aquatic Microbial Ecology*, *57*, 203–220. https://doi.org/10.3354/ame01334

Graham, R. M., De Boer, A. M., van Sebille, E., Kohfeld, K. E., & Schlosser, C. (2015). Inferring source regions and supply mechanisms of iron in the Southern Ocean from satellite chlorophyll data. *Deep-Sea Research Part I: Oceanographic Research Papers*, *104*, 9–25. https://doi.org/10.1016/j.dsr.2015.05.007

Grenier, M., Della Penna, A., & Trull, T. W. (2015). Autonomous profiling float observations of the high-biomass plume downstream of the Kerguelen plateau in the Southern Ocean. *Biogeosciences*, *12*(9), 2707–2735. https://doi.org/10.5194/bg-12-2707-2015

Heywood, K. J., Sparrow, M. D., Brown, J., & Dickson, R. R. (1999). Frontal structure and Antarctic bottom water flow through the Princess Elizabeth trough, Antarctica. *Deep-Sea Research Part I: Oceanographic Research Papers*, *46*(7), 1181–1200. https://doi.org/10.1016/S0967-0637(98)00108-3

Jickells, T. D., An, Z. S., Andersen, K. K., Baker, A. R., Bergametti, G., Brooks, N., et al. (2005). Global iron connections between desert dust, ocean biogeochemistry, and climate. *Science*, *308*(5718), 67–71. https://doi.org/10.1126/science.1105959

Johnson, R., Strutton, P. G., Wright, S. W., McMinn, A., & Meiners, K. M. (2013). Three improved satellite chlorophyll algorithms for the Southern Ocean. *Journal of Geophysical Research: Oceans*, *118*, 3694–3703. https://doi.org/10.1002/jgrc.20270

de Jong, J., Schoemann, V., Lannuzel, D., Croot, P., de Baar, H., & Tison, J.-L. (2012). Natural iron fertilization of the Atlantic sector of the Southern Ocean by continental shelf sources of the Antarctic Peninsula. *Journal of Geophysical Research*, *117*, G01029. https://doi.org/10.1029/2011JG001679

de Jong, J., Stammerjohn, S. E., Ackley, S. F., Tison, J.-L., Mattielli, N., & Schoemann, V. (2015). Sources and fluxes of dissolved iron in the Bellingshausen Sea (West Antarctica): The importance of sea ice, icebergs and the continental margin. *Marine Chemistry*, *177*, 518–535. https://doi.org/10.1016/j.marchem.2015.08.004

Karsh, K. L., Trull, T. W., Lourey, M., & Sigman, D. M. (2003). Relationship of nitrogen isotope fractionation to phytoplankton size and iron availability during the Southern Ocean Iron RElease Experiment (SOIREE). *Limnology and Oceanography*, *48*(3), 1058–1068. https://doi.org/10.4319/lo.2003.48.3.1058

Klunder, M. B., Laan, P., Middag, R., De Baar, H., & van Ooijen, J. C. (2011). Dissolved iron in the Southern Ocean (Atlantic sector). *Deep-Sea Research Part II: Topical Studies in Oceanography*, *58*(25-26), 2678–2694. https://doi.org/10.1016/j.dsr2.2010.10.042

Lagerström, M. E., Field, M. P., Séguret, M., Fischer, L., Hann, S., & Sherrell, R. M. (2013). Automated on-line flow-injection ICP-MS determination of trace metals (Mn, Fe, Co, Ni, Cu and Zn) in open ocean seawater: Application to the GEOTRACES program. *Marine Chemistry*, *155*, 71–80. https://doi.org/10.1016/j.marchem.2013.06.001

Lannuzel, D., Vancoppenolle, M., van der Merwe, P., de Jong, J., Meiners, K. M., Grotti, M., et al. (2016). Iron in sea ice: Review and new insights. *Elementa*, *4*, 1–19.

Mahadevan, A. (2016). The impact of submesoscale physics on primary productivity of plankton. *Annual Review of Marine Science*, *8*, 17.1–17.24.

Marsay, C. M., Sedwick, P. N., Dinniman, M. S., Barrett, P. M., Mack, S. L., & McGillicuddy, D. J. Jr. (2014). Estimating the benthic efflux of dissolved iron on the Ross Sea continental shelf. *Geophysical Research Letters*, *41*, 7576–7583. https://doi.org/10.1002/2014GL061684

Martin, J. (1990). Glacial-interglacial CO_2 change: The iron hypothesis. *Paleoceanography*, *5*(1), 1–13. https://doi.org/10.1029/PA005i001p00001

McCartney, M. S., & Donohue, K. A. (2007). A deep cyclonic gyre in the Australian–Antarctic Basin. *Progress in Oceanography*, *75*(4), 675–750. https://doi.org/10.1016/j.pocean.2007.02.008

Mock, T., & Hoch, N. (2005). Long-term temperature acclimation of photosynthesis in steady-state cultures of the polar diatom Fragilariopsis cylindrus. *Photosynthesis Research*, *85*, 307–317.

Mongin, M., Abraham, E. R., & Trull, T. W. (2009). Winter advection of iron can explain the summer phytoplankton bloom that extends 1000 km downstream of the Kerguelen plateau in the Southern Ocean. *Journal of Marine Research*, *67*(2), 225–237. https://doi.org/10.1357/002224009789051218

Mongin, M., Molina, E., & Trull, T. W. (2008). Seasonality and scale of the Kerguelen plateau phytoplankton bloom: A remote sensing and modeling analysis of the influence of natural iron fertilization in the Southern Ocean. *Deep-Sea Research Part II: Topical Studies in Oceanography*, *55*(5–7), 880–892. https://doi.org/10.1016/j.dsr2.2007.12.039

Moore, J., & Abbott, M. (2002). Surface chlorophyll concentrations in relation to the Antarctic Polar Front: Seasonal and spatial patterns from satellite observations. *Journal of Marine Systems*, *37*(1-3), 69–86. https://doi.org/10.1016/S0924-7963(02)00196-3

Moore, J. K., Doney, S. C., Glover, D. M., & Fung, I. Y. (2002). Iron cycling and nutrient-limitation patterns in surface waters of the World Ocean. *Deep-Sea Research Part II: Topical Studies in Oceanography*, *49*, 463–507.

Orsi, A. H., Whitworth, T. III, & Nowlin, W. D. Jr. (1995). On the meridional extent and fronts of the Antarctic Circumpolar Current. *Deep-Sea Research Part I: Oceanographic Research Papers*, *42*(5), 641–673. https://doi.org/10.1016/0967-0637(95)00021-W

Park, Y.-H., Fuda, J.-L., Durand, I., & Naveira Garabato, A. C. (2008). Internal tides and vertical mixing over the Kerguelen plateau. *Deep-Sea Research Part II: Topical Studies in Oceanography*, *55*(5-7), 582–593. https://doi.org/10.1016/j.dsr2.2007.12.027

Park, Y.-H., Vivier, F., Roquet, F., & Kestenare, E. (2009). Direct observations of the ACC transport across the Kerguelen plateau. *Geophysical Research Letters*, *36*, L18603. https://doi.org/10.1029/2009GL039617

Pellichero, V., Sallee, J.-B., Schmidtko, S., Roquet, F., & Charrassin, J.-B. (2017). The ocean mixed layer under Southern Ocean sea-ice: Seasonal cycle and forcing. *Journal of Geophysical Research: Oceans*, *122*, 1608–1633. https://doi.org/10.1002/2016JC011970

Quéroué, F., Sarthou, G., Planquette, H. F., Bucciarelli, E., Chever, F., van der Merwe, P., et al. (2015). High variability in dissolved iron concentrations in the vicinity of the Kerguelen Islands (Southern Ocean). *Biogeosciences*, *12*(12), 3869–3883. https://doi.org/10.5194/bg-12-3869-2015

R Core Team (2016). R: A language and environment for statistical computing version 3.3.2. R Foundation for Statistical Computing, Vienna, Austria. Retrieved from https://www.r-project.org/

Raymond, B. (2014). Polar environmental data layers Australian Antarctic Data Centre—CAASM. Metadata at https://data.aad.gov.au/metadata/records/Polar_Environmental_Data

Rintoul, S., Sokolov, S., & Massom, R. (2008). Rapid development and persistence of a massive Antarctic sea ice tongue. *Journal of Geophysical Research*, *113*, C07045. https://doi.org/10.1029/2007JC004541

Robinson, J., Popova, E. E., Srokosz, M. A., & Yool, A. (2016). A tale of three islands: Downstream natural iron fertilization in the Southern Ocean. *Journal of Geophysical Research: Oceans*, *121*, 3350–3371. https://doi.org/10.1002/2015JC011319

Roquet, F., Park, Y.-H., Guinet, C., Bailleul, F., & Charrassin, J. B. (2009). Observations of the Fawn Trough Current over the Kerguelen plateau from instrumented elephant seals. *Journal of Marine Systems*, *78*(3), 377–393. https://doi.org/10.1016/j.jmarsys.2008.11.017

Rosenberg, M., & Eriksen, R. (2016). *Aurora Australis Marine Science Cruise AU1603—Oceanographic field measurements and analysis* (pp. 1–33). Hobart, AU: Antarctic Climate and Ecosystems Cooperative Research Centre.

Schallenberg, C., van der Merwe, P., Chever, F., Cullen, J. T., Lannuzel, D., & Bowie, A. R. (2016). Dissolved iron and iron (II) distributions beneath the pack ice in the East Antarctic (120°E) during the winter spring/transition. *Deep-Sea Research Part II: Topical Studies in Oceanography*, *131*, 96–110. https://doi.org/10.1016/j.dsr2.2015.02.019

Sedwick, P., & DiTullio, G. (1997). Regulation of algal blooms in Antarctic shelf waters by the release if iron from melting sea ice. *Geophysical Research Letters*, *24*(20), 2515–2518. https://doi.org/10.1029/97GL02596

Sherrell, R. M., Annett, A. L., Fitzsimmons, J. N., Roccanova, V. J., & Meredith, M. P. (2018). A 'shallow bathtub ring' of local sedimentary iron input maintains the Palmer Deep biological hotspot on the West Antarctic Peninsula shelf. *Philosophical Transactions of the Royal Society A*, *376*(2122), 20170171. https://doi.org/10.1098/rsta.2017.0171

Sigman, D., & Boyle, E. (2000). Glacial/interglacial variations in atmospheric carbon dioxide. *Nature*, *407*(6806), 859–869. https://doi.org/10.1038/35038000

Smith, W. O., & Nelson, D. M. (1985). Phytoplankton bloom produced by a receding ice edge in the Ross Sea: Coherence with the density field. *Science*, *227*(4683), 163–166. https://doi.org/10.1126/science.227.4683.163

Sokolov, S., & Rintoul, S. (2007). On the relationship between fronts of the Antarctic Circumpolar Current and surface chlorophyll concentrations in the Southern Ocean. *Journal of Geophysical Research*, *112*, C07030. https://doi.org/10.1029/2006JC004072

Sparrow, M. D., Heywood, K. J., Brown, J., & Stevens, D. P. (1996). Current structure of the south Indian Ocean. *Journal of Geophysical Research*, *101*(C3), 6377–6391. https://doi.org/10.1029/95JC03750

Sumner, M. D. (2016). Raadtools: Tools for synoptic environmental spatial data. R package version 0.4.0.9001. Retrieved from https://github.com/AustralianAntarcticDivision/raadtools

Sumner, M. D. (2017). Roc: Working with ocean colour data. R package version 0.0.8.9001. Retrieved from https://github.com/mdsumner/roc

Tagliabue, A., Sallée, J. B., Bowie, A. R., Lévy, M., Swart, S., & Boyd, P. W. (2014). Surface-water iron supplies in the Southern Ocean sustained by deep winter mixing. *Nature Geoscience*, *7*(4), 314–320. https://doi.org/10.1038/NGEO2101

Trull, T. W., Davies, D., & Casciotti, K. (2008). Insights into nutrient assimilation and export in naturally iron-fertilized waters of the Southern Ocean from nitrogen, carbon and oxygen isotopes. *Deep-Sea Research Part II: Topical Studies in Oceanography*, *55*(5-7), 820–840. https://doi.org/10.1016/j.dsr2.2007.12.035

Trull, T. W., Davies, D., Dehairs, F., Cavagna, A.-J., Lasbleiz, M., Laurenceau-Cornec, E. C., et al. (2015). Chemometric perspectives on plankton community responses to natural iron fertilization over and downstream of the Kerguelen plateau in the Southern Ocean. *Biogeosciences*, *12*(4), 1029–1056. https://doi.org/10.5194/bg-12-1029-2015

Tynan, C. T. (1998). Ecological importance of the southern boundary of the Antarctic Circumpolar Current. *Nature*, *392*(6677), 708–710. https://doi.org/10.1038/33675

Vancoppenolle, M., Meiners, K. M., Michel, C., Bopp, L., Brabant, F., Carnat, G., et al. (2013). Role of sea ice in global biogeochemical cycles: Emerging views and challenges. *Quaternary Science Reviews*, *79*, 207–230. https://doi.org/10.1016/j.quascirev.2013.04.011

van der Merwe, P., Bowie, A. R., Quéroué, F., Armand, L., Blain, S., Chever, F., et al. (2015). Sourcing the iron in the naturally-fertilised bloom around the Kerguelen plateau: Particulate trace metal dynamics. *Biogeosciences*, *12*(3), 739–755. https://doi.org/10.5194/bg-12-739-2015

Vivier, F., Park, Y.-H., Sekma, H., & Le Sommer, J. (2015). Variability of the Antarctic Circumpolar Current transport through the Fawn Trough, Kerguelen plateau. *Deep-Sea Research Part II: Topical Studies in Oceanography*, *114*, 12–26. https://doi.org/10.1016/j.dsr2.2014.01.017

Wadley, M. R., Jickells, T. D., & Heywood, K. J. (2014). The role of iron sources and transport for Southern Ocean productivity. *Deep-Sea Research Part II: Topical Studies in Oceanography*, *87*, 82–94. https://doi.org/10.1016/j.dsr.2014.02.003

Wakatsuchi, M., Ohshima, K. I., Hishida, M., & Naganobu, M. (1994). Observations of a street of cyclonic eddies in the Indian Ocean sector of the Antarctic Divergence. *Journal of Geophysical Research*, *99*(C10), 20,417–20,426. https://doi.org/10.1029/94JC01478

Wright, S. W., van den Enden, R. L., Pearce, I., Davidson, A. T., Scott, F. J., & Westwood, K. J. (2010). Phytoplankton community structure and stocks in the Southern Ocean (30–80°E) determined by CHEMTAX analysis of HPLC pigment signatures. *Deep-Sea Research Part II: Topical Studies in Oceanography*, *57*(9–10), 758–778. https://doi.org/10.1016/j.dsr2.2009.06.015